RSC Advances

Fabrication of nano-sized Ag2CO3/RGO photocatalyst with enhanced visible-light photocatalytic activity and stability

Journal:	*RSC Advances*
Manuscript ID:	RA-ART-05-2014-004792.R2
Article Type:	Paper
Date Submitted by the Author:	07-Jul-2014
Complete List of Authors:	Daopeng, Dai; Hubei University of arts and science, Suqin, Liu; Hubei University of arts and science, Ying, Liang; Hubei University of arts and science, Ke, Liu; Hubei University of arts and science,

Cite this: DOI: 10.1039/c0xx00000x

www.rsc.org/xxxxxx

ARTICLE TYPE

Fabrication of nano-sized Ag_2CO_3/reduced graphene oxide photocatalyst with enhanced visible-light photocatalytic activity and stability

Gaopeng Dai,* [a,b] Suqin Liu,[a,b] Ying Liang[a] and Ke Liu[b]

Received (in XXX, XXX) Xth XXXXXXXXX 20XX, Accepted Xth XXXXXXXXX 20XX

DOI: 10.1039/b000000x

Nano-sized Ag_2CO_3 and reduced graphene oxide (RGO) composites were fabricated by a facile chemical precipitation approach in N,N-dimethylformamide (DMF) solvent. The as-prepared Ag_2CO_3/RGO nanocomposites were characterized by X-ray diffraction pattern (XRD), Raman spectroscopy, X-ray photoelectron spectroscopy (XPS), scanning electron microscopy (SEM), transmission electron microscopy (TEM), and ultraviolet-visible (UV-vis) diffuse reflectance spectroscopy (DRS). The photocatalytic activity of the samples was evaluated by photocatalytic degradation of methyl orange (MO) under visible light irradiation. The results showed that the nano-sized Ag_2CO_3 particles are deposited on the surfaces of RGO. The Ag_2CO_3/RGO nanocomposites exhibited much higher photocatalytic activity than the pure nano-sized Ag_2CO_3 due to the improved separation efficiency of photogenerated carriers, and Ag_2CO_3/2 wt% RGO displayed the highest photocatalytic degradation efficiency. Furthermore, the photocatalytic and structural stability of Ag_2CO_3 is greatly enhanced due to the good electron transfer of RGO.

1. Introduction

Photocatalytic degradation of organic pollutants by using semiconductor photocatalysts is of growing interest for water purification.[1-4] Among these materials, titanium dioxide (TiO_2) is the most widely used photocatalyst because of its large availability, low cost, nontoxicity, and relatively high chemical stability.[5,6] However, due to the large band gap (3.2 eV), TiO_2 is mainly catalytically active under UV light irradiation, which merely accounts for ca. 4.5% of solar energy.[7,8] Considering energy saving and utilization, sunlight or visible-light (which accounts for ca. 45% of solar energy), is the most promising energy source for the operation of the photocatalysts. Therefore, it is desirable to develop novel photocatalysts that can utilize visible light under sunlight irradiation. Recently, silver-containing compounds have been demonstrated to be efficient photocatalytic materials under visible-light irradiation.[9-14] For example, Hu and co-workers reported fabrication of monoclinic structural Ag_3VO_4 and its visible-light photocatalytic activity for the decolorization of azodye acid red B.[9] Singh et al. reported synthesis of illmenite $AgSbO_3$ by ion-exchange reaction of $NaSbO_3$ with silver nitrate, which showed visible-light photocatalytic activity for the decomposition of methylene blue, rhodamine B, and 4-chlorophenol.[10] Huang and co-workers reported that silver halides exhibit high visible-light photocatalytic activity and photostability due to the plasmon resonance of Ag nanoparticles formed on the surface of silver halide particles.[11] Ye et al. reported that the Ag_3PO_4 photocatalyst exhibits extremely high photocatalytic capabilities in the oxidation of water and in the photodecomposition of organic contaminants in aqueous solution under visible-light irradiation.[12] Wang and co-workers found that crystalline Ag_2O particles can be used as an efficient photocatalyst for the decomposition of methyl orange (MO) under visible-light irradiation.[13] Tang et al. reported the synthesis of novel $AgIO_4$ semiconductor, which shows much higher activity than Ag_3PO_4 or Ag_3AsO_4.[14] Very recently, it was reported that Ag_2CO_3 crystal exhibited universal high-efficient photodegradation performance for (rhodamine B, methylene blue, MO) and phenol.[15-17] However, Ag_2CO_3 is unstable. The transformation of Ag^+ into Ag usually takes place due to the combination of the photo-induced electron and interstitial Ag^+ during the photocatalytic process, which results in the photocorrosion of Ag_2CO_3 in the absence of electron acceptors.[15]

Reduced graphene oxide (RGO), as a two-dimensional single-layer carbon sheet, has attracted great interest for photocatalytic applications because of its unique properties, such as a large theoretical specific surface area, superior mobility of charge carriers, and good chemical stability.[18-21] The ability of graphene to transfer electrons can lengthen the lifetime of photoexcited electrons, which can suppress the recombination of photoexcited electrons and holes.[22] For the moment, Ag_2CO_3/ Graphene oxide (GO) composites have been synthesized to improve the structural stability and photocatalytic activity of Ag_2CO_3.[23] It is reported that the electrical conductivity was improved after GO was reduced,[24] and the high electrical conductivity is beneficial to transferring of the photogenerated electrons.[25] However, there has no work focusing on preparing Ag_2CO_3/RGO composites for degrading organic pollutants under the visible light. Moreover, the particle size of Ag_2CO_3 remains relatively large, hindering its performance in photocatalytic

processes. It is widely accepted that a large surface area of the catalyst enhances the photocatalytic activity of photocatalyst because a high surface area increases the number and density of redox reaction sites.[26] Considering the remarkable properties of RGO, the limitations of the Ag_2CO_3 photocatalytic system and the higher surface area of nanoparticles than microparticles, the combination of RGO and nano-sized Ag_2CO_3 could be regarded as an ideal strategy to construct stable and efficient composite photocatalyst.

In this work, we, for the first time, synthesized Ag_2CO_3/RGO nanocomposites by a chemical precipitation method. It is found that the obtained nano-sized Ag_2CO_3/RGO photocatalysts showed remarkably enhanced photocatalytic activities toward degradation of MO in comparison with pure nano-sized Ag_2CO_3 under visible light. More importantly, the addition of RGO could enhance the photocatalytic stability of Ag_2CO_3.

2. Experimental

2.1. Sample preparation

All reagents used in this study were of analytical grade and were purchased from Shanghai Chemical Reagent Factory of China without further purification. Graphene oxide (GO) was prepared by a modified Hummers method[27] and reduced graphene oxide (RGO) was obtained by a chemical reduction of GO using sodium borohydride.[28] Typically, 100 mg of GO was exfoliated in 200 mL of distilled water by ultra-sonication for 3 h to form a homogeneous brown GO colloidal dispersion with a concentration. Subsequently, 1.135 g of $NaBH_4$ was added into the above GO solution under vigorous stirring. After the mixture was stirred for 3 h at 80 °C, the obtained precipitates were separated by centrifuge followed by washing with distilled water for several times. The product was then dried in a vacuum oven at 40 °C.

For synthesis of nano-sized Ag_2CO_3/RGO composite, a certain amount of the RGO was dispersed into 30 mL of N,N-dimethylformamide (DMF) with sonicating for 2 h to form the dispersion of RGO. Subsequently, 3 mmol of $AgNO_3$ was added into the dispersion of RGO under vigorous stirring. After stirring for 10 min, 3 mmol of K_2CO_3 dissolved in 15 mL of mixed solution of ethanol and water (volume ratio, 1:1) was then added dropwise into the above dispersion under magnetically stirring. The mixture was stirred for 20 min. The obtained precipitates were then washed with distilled water and ethanol for several times, respectively. Finally, powdered sample was obtained after drying in a vacuum oven at 60 °C. The contents of adding RGO are 2, 4, 8, and 12 mg, and the obtained samples are labeled as Ag_2CO_3/0.5 wt% RGO, Ag_2CO_3/1 wt% RGO, Ag_2CO_3/2 wt% RGO, and Ag_2CO_3/3 wt% RGO, respectively. For comparison purpose, pure Ag_2CO_3 nanoparticles were synthesized without the addition of RGO. Micro-sized Ag_2CO_3 and N-doped TiO_2 were synthesized by previously reported methods,[15,29] respectively.

2.2 Characterization

X-ray diffraction (XRD) patterns were obtained on a D/MAX-RB X-ray diffractometer (Rigaku, Japan) using Cu Kα radiation at a scan rate (2θ) of 0.05° s^{-1}. Scanning electron microscopy (SEM) were performed in an S-4800 Field Emission SEM (FESEM, Hitachi, Japan) at an accelerating voltage of 10 kV. Transmission electron microscopy (TEM) analyses were conducted with a JEM-2100F electron microscope (JEOL, Japan) operating at 200 kV. Raman spectra were acquired on a Reflex Raman Microprobe (Renishaw inVia, England). X-ray photoelectron spectroscopy (XPS) measurements were performed on a VG ESCALAB MKII XPS system with an Mg Kα source and a charge neutralizer. The UV-visible diffuse reflectance spectra were obtained using a UV-visible spectrophotometer (UV-2550, Shimadzu, Japan). Fine $BaSO_4$ powder was used as a standard.

2.3. Photocatalytic Evaluation

The photocatalytic activity of the as-prepared sample was measured for the photocatalytic oxidation of methyl orange (MO) under visible-light at ambient temperature. Briefly, 0.1 g of Ag_2CO_3/RGO sample was dispersed in a 25 mL of 4 $\times 10^{-5}$ M MO aqueous solution in a 7.0 cm culture dish. Prior to illumination, the resulting mixture was allowed to reach the adsorption-desorption equilibrium. A 200 W xenon lamp with a 420 nm cutoff filter positioned 25 cm above the dish was used as a visible-light source to trigger the photocatalytic reaction. The concentration of MO was determined by an UV-visible spectrophotometer (UV-2550, Shimadzu, Japan). After irradiation for certain time, the reaction solution was sampled to measure the concentration change of MO. For comparison, the photocatalytic activity of N-doped TiO_2 counterparts was also measured.

3. Results and discussion

3.1. Structures and morphology

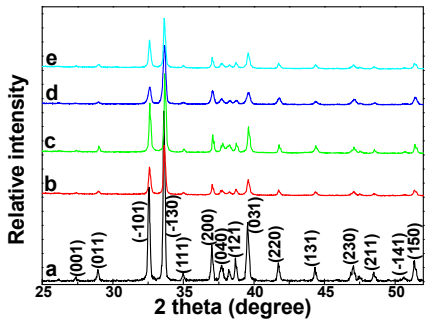

Fig. 1 XRD patterns of micro-sized Ag_2CO_3 (a), nano-sized Ag_2CO_3 (b), Ag_2CO_3/0.5 wt% RGO (c), Ag_2CO_3/1 wt% RGO (d), and Ag_2CO_3/3 wt% RGO (e) composites.

XRD analysis (Fig.1) shows that all the diffraction peaks of the as-prepared samples were in good agreement with those of the monoclinic structure of Ag_2CO_3 (JCPDS file No. 26-0339). The XRD peak intensities of the nano-sized Ag_2CO_3 are weaker than that of the micro-sized Ag_2CO_3, and the width of all diffraction peaks is broader than that of the micro-sized Ag_2CO_3 sample, suggesting the formation of smaller Ag_2CO_3 crystallites in nano-sized Ag_2CO_3. This was attributed to the synergic performance of DMF and ethanol.[20,30] In DMF solvent, the Ag^+ ions and DMF could form the weekly bound $[Ag(amide)]^+$ complex.[20] When the CO_3^{2-} ions in ethanol and water were added into the above DMF

solvent, strong chemical combination occurred between the Ag^+ ions in the $[Ag(amide)]^+$ complex and CO_3^{2-} ions, resulting in the formation of Ag_2CO_3 particles. The bound DMF in $[Ag(amide)]^+$ complex and ethanol, which was acted as a capping agent,[28] can hinder the growth of Ag_2CO_3 crystal, leads to the formation of Ag_2CO_3 nanoparticles. Fig. S1 shows that peak of RGO at around $2\theta = 10.2^o$ corresponds to the (001) reflection. However, no peak attributed to RGO was observed in the XRD pattern, which may be attributed to the destruction of the regular stacking of graphene sheets by the loading of Ag_2CO_3 nanoparticles.[31,32]

The presence of RGO and Ag_2CO_3 are further supported by Raman spectroscopy. As is shown in Fig.2, two characteristic peaks of RGO can be observed, the G-band, which is due to the E_{2g} vibrational mode of sp^2 bonded carbon and is observed at 1580 cm^{-1}, and the D-band at 1350 cm^{-1} is due to the A_{1g} mode breathing vibrations of six-membered sp^2 carbon rings. The Raman spectra of Ag_2CO_3 display four characteristic peaks located at approximately 959 cm^{-1}, 1012 cm^{-1}, 1120 cm^{-1}, 1170 cm^{-1}. Besides the bands attributed to the Ag_2CO_3 vibrations, two characteristic peaks for the graphitized structures are observed in the Raman spectrum of Ag_2CO_3/RGO composite, suggesting the existence of RGO in the Ag_2CO_3/RGO composite.

Fig. S 3 shows the whole XPS spectrum of the Ag_2CO_3/2 wt% RGO composite. In the high-resolution XPS spectrum of Ag 3d, two individual peaks at about 368.1 and 374.0 eV can be assigned to Ag $3d_{5/2}$ and Ag $3d_{3/2}$ binding energies, respectively, which is characteristic of Ag^+ in Ag_2CO_3.[33] The peaks centered at 284.8, 286.2, 288, and 289.1 eV in Fig. S3c can be attributed to C-C, C-O, C= O and O=C-O groups, respectively. The peaks at 531.5, 532.6, and 533.3 eV in Fig. S3d consist with the characteristic peaks of oxygen in Ag_2CO_3, O-C, and O=C-O, respectively.

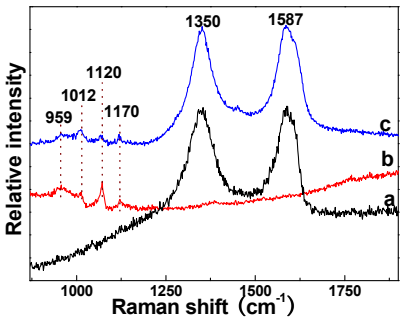

Fig. 2 Raman spectra of RGO (a) pure Ag_2CO_3 (b) and Ag_2CO_3/2 wt% RGO (c) composite.

The morphology of the as-prepared samples was investigated using SEM. RGO exhibits flaky foam-like structures (Fig. S2). Fig. 3 shows the SEM images of the micro-sized, nano-sized Ag_2CO_3 and Ag_2CO_3/RGO samples. In contrast to the micro-sized Ag_2CO_3 particles with an average size of ca. 2-4 μm (Fig. 3a), the particle size of the nano-sized Ag_2CO_3 (Fig. 3b) and Ag_2CO_3/1 wt% RGO (Fig. 3c) samples decreases sharply, indicating that the DMF and ethanol play dominant roles in the formation of nano-sized Ag_2CO_3. This is in a good agreement with the above XRD results. The particle size of the nano-sized Ag_2CO_3 and Ag_2CO_3/RGO samples is ca. 100 nm. A further observation indicates that Ag_2CO_3 nanoparticles were attached on the surface of RGO in the Ag_2CO_3/RGO sample. It is reported that the hydrophobic RGO can be well dispersed in DMF,[34,35] and RGO has large specific surface area, which facilitates the absorption of Ag^+ ions by the oxygen-containing functional groups (COOH, C–OH, and C–O–C) on the surface of RGO. When CO_3^{2-} ions were added into the dispersion, Ag_2CO_3 nanoparticles could grow on the surface of RGO and the desired Ag_2CO_3/RGO nanocomposite were obtained. The TEM image (Fig. 3d and 3e) show that RGO exhibits a large size and flat structure and the well-dispersed Ag_2CO_3 nanoparticles adhere to the surface of RGO closely. The results are in good agreement with the SEM images.

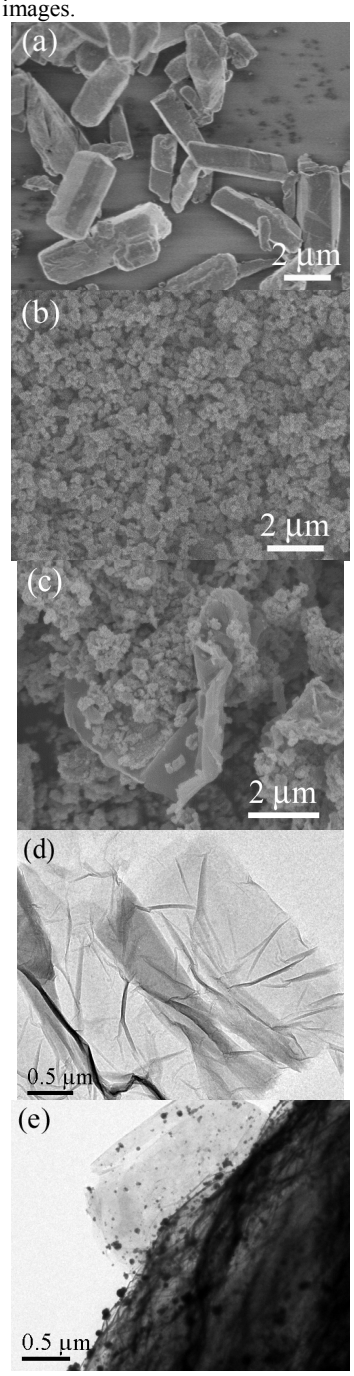

Fig. 3 SEM (a,b,c) and TEM (d,e) images of micro-sized Ag_2CO_3 (a), nano-sized Ag_2CO_3 (b,d), Ag_2CO_3/2 wt% RGO (c,e).

3.2. Optical properties

The light-absorbance property of nano-sized Ag_2CO_3 and Ag_2CO_3/RGO composites was probed with UV–vis absorption spectra, as shown in Fig. 4. Pure Ag_2CO_3 shows a sharp fundamental absorption edge at about 480 nm. Compared with the spectrum of Ag_2CO_3, there is an obvious enhanced absorbance in the visible-light region when Ag_2CO_3 was incorporated with RGO, and the absorption increases with the increase of RGO content in the Ag_2CO_3/RGO composites.

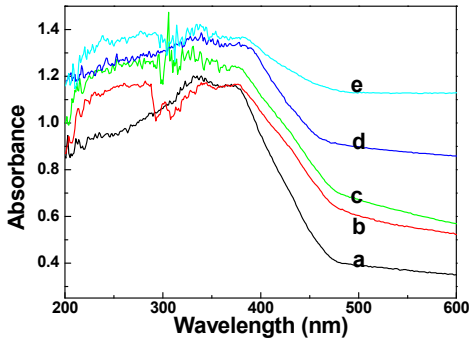

Fig. 4 UV–Vis absorption spectra of nano-sized Ag_2CO_3 (a), Ag_2CO_3/0.5 wt% RGO (b), Ag_2CO_3/1 wt% RGO (c) Ag_2CO_3/2 wt% RGO (d) and Ag_2CO_3/3 wt% RGO (e) composites.

3.3. Photocatalytic activity

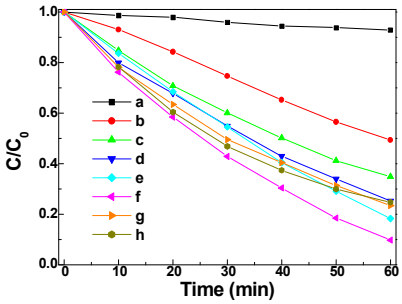

Fig. 5 Photocatalytic degradation curves of MO over N-TiO_2 (a), Micro-sized Ag_2CO_3 (b) nano-sized Ag_2CO_3 (c), Ag_2CO_3/0.5 wt% RGO (d), Ag_2CO_3/2 wt% RGO (f), Ag_2CO_3/3 wt% RGO (g) and Ag_2CO_3/1 wt% GO (h) composites under visible light irradiation.

The photocatalytic activity of the prepared samples was evaluated by photocatalytic decolorization of MO aqueous solution under visible light. Temporal concentration changes of MO were monitored by examining the variations in maximal absorption in UV-vis spectra at 464 nm. In the dark, almost no change in the concentration of MO was observed in the presence of Ag_2CO_3/RGO. Furthermore, illumination in the absence of Ag_2CO_3/RGO did not result in the photocatalytic decolorization of MO. Fig. 5 shows a comparison of photocatalytic activities of the Ag_2CO_3/RGO composites. After 60 min of irradiation, the photocatalytic decomposition of MO by micro-sized and nano-sized Ag_2CO_3 was up to 51% and 66%, respectively; however, only a little MO was decomposed by N-doped TiO_2 under the same condition. Nano-sized Ag_2CO_3 exhibits a higher visible-light photocatalytic activity than micro-sized Ag_2CO_3 due to the higher specific surface area of nanoparticles than microparticles. Further observation shows that the RGO content has a great effect on the photocatalytic activity of Ag_2CO_3. The pure Ag_2CO_3 sample shows a poor photocatalytic activity compared with that of Ag_2CO_3/RGO composites. A small amount of RGO could lead to a sharp increase of MO decomposition from 9% to 25%. Ag_2CO_3/2 wt% RGO nanocomposite shows the best photocatalytic degradation ability among these Ag_2CO_3/RGO composites with various RGOs contents. About 91% MO was decomposed by Ag_2CO_3/2 wt% RGO after 60 min of irradiation. The photocatalytic activity of Ag_2CO_3/2 wt% RGO composite is also higher than the corresponding Ag_2CO_3/2 wt% GO sample. The higher activity may be attributed to the high electrical conductivity of RGO, which is beneficial to transferring of the photogenerated electrons, and then improving the separation of photoinduced carriers.

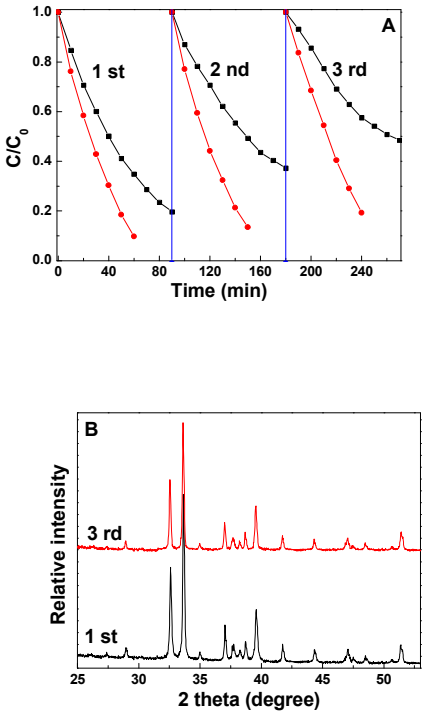

Fig. 6 (A) Repeated photocatalytic degradation of MO solution under visible light irradiation (square: nano-sized Ag_2CO_3; circle: Ag_2CO_3/2 wt% RGO composite); (B) XRD patterns of Ag_2CO_3/2 wt% RGO composite after the first and third cycle experiments.

To compare the photocatalytic stability of the pure nano-sized Ag_2CO_3 and Ag_2CO_3/RGO composites, the used pure Ag_2CO_3 nanoparticles and Ag_2CO_3/RGO nanocomposite were collected and reused in three successive MO degradation

experiments, respectively. As shown in Fig. 6A, the photocatalytic activity of Ag_2CO_3/2 wt% RGO is decreased slowly in three successive experimental runs. However, the rate of MO degradation for pure Ag_2CO_3 decreases more significantly in three successive experimental runs under the same conditions. This result indicates that the Ag_2CO_3/RGO nanocomposites are more stable than the pure Ag_2CO_3 nanoparticles. The used Ag_2CO_3/2 wt% RGO was further collected after three cycle times and characterized by XRD. It was also showed that the photocatalyst treatment after the recycling experiment had no significant effect on the structure of the Ag_2CO_3/2 wt% RGO sample (Fig. 6B). The results further confirm the enhanced stability of Ag_2CO_3/RGO composites.

The enhanced photocatalytic activity and stability of Ag_2CO_3/RGO composite could be ascribed to the ability of RGO to separate and transfer electron–hole pairs efficiently. As shown in Fig. 7, under visible light irradiation, electrons (e^-) in the valence band (VB) of Ag_2CO_3 can be excited to its conduction band (CB), causing the generation of holes (h^+) in the VB of Ag_2CO_3 simultaneously. Because of the presence of conductive RGO, it can serve as an effective acceptor of the photoexcited electrons; hence, the photogenerated CB electrons of Ag_2CO_3 can be transferred to RGO in the Ag_2CO_3/RGO composites. The transportation and mobility of electrons on RGO are very rapid in the specific π-conjugated structure; thus the efficient electron transfer from Ag_2CO_3 to RGO keeps electrons away from the Ag_2CO_3. More photogenerated electrons and holes are produced by continuously working in this way, effectively suppressing the charge recombination and improving the photocatalytic activity, which reduces the decomposition rates of Ag^+ to metallic Ag in the photocatalytic process, resulting in a better stability of Ag_2CO_3/RGO composites in the photocatalytic process.

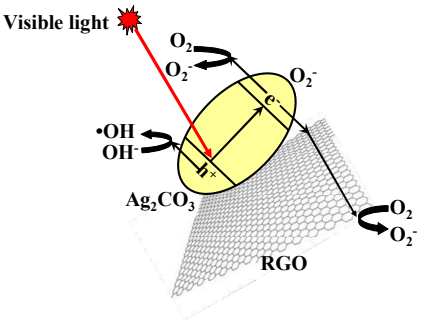

Fig. 7 Schematic diagram for the charge separation at a visible-light irradiated Ag_2CO_3/RGO system

4. Conclusions

The nano-sized Ag_2CO_3/RGO composites have been successfully and directly produced via a facile chemical precipitation approach in DMF solvent. The Ag_2CO_3/RGO nanocomposites exhibited higher photocatalytic activity and stability than that of the pure nano-sized Ag_2CO_3 for the degradation of MO, and Ag_2CO_3/2 wt% RGO exhibited the highest photocatalytic degradation efficiency. The enhanced photocatalytic activity and stability can be mainly attributed to the existence of RGO, which can accelerate the charge separation, transportation and transfer.

Acknowledgements

This work was financially supported by the Natural Science Foundation of Hubei Province (2012FFB01903), Research Program of Hubei Province Department of Education (Q20132508), and Science and Technology Bureau of Xiangyang.

Notes and references

[a] *Department of chemical engineering and food science, Hubei University of arts and science, Xiangyang 441053, P. R. China. Tel: 0086-710-3592609; Email: dgp2000@126.com*

[b] *Hubei key laboratory of low dimensional optoelectronic materials and devices, Xiangyang 441053, P. R. China. E-mail: 15869645@qq.com*

† Electronic Supplementary Information (ESI) available: [details of any supplementary information available should be included here]. See DOI: 10.1039/b000000x/

‡ Footnotes should appear here. These might include comments relevant to but not central to the matter under discussion, limited experimental and spectral data, and crystallographic data.

1 A. Kudo and Y. Miseki, *Chem. Soc. Rev.*, 2009, **38**, 253-278.
2 S. W. Liu, J. G. Yu and M. Jaroniec, *J. Am. Chem. Soc.*, 2010, **132**, 11914-11916.
3 G. P. Dai, S. Q. Liu, Y. Liang, H. J. Liu and Z. C. Zhong, *J. Mol. Catal. A: Chem.*, 2013, **368-369**, 38-42.
4 X. Xu, X. P. Shen, G. X. Zhu, L. Q. Jing, X. S. Liu and K. M. Chen, *Chem. Eng. J.*, 2012, **200-202**, 521-531.
5 G. Cappelletti, C. L. Bianchi and S. Ardizzone, *Appl. Catal. B*, 2008, **78**, 193-201.
6 S. W. Liu, J. G. Yu and M. Jaroniec, *Chem. Mater.*, 2011, **23**, 4085-4093.
7 C. Chen, W. Ma and J. Zhao, *Chem. Soc. Rev.*, 2010, **39**, 4206-4219.
8 A. Kubacka, M. Fernandez-García and G. Colón, *Chem. Rev.*, 2011, **112**, 1555-1614.
9 X. X. Hu, C. Hu and J. H. Qu, *Mate. Res. Bull.*, 2008, **43**, 2986-2997.
10 J. Singh and S. Uma, *J. Phys. Chem. C*, 2009, **113**, 12483-12488.
11 P. Wang, B. B. Huang, X. Y. Qin, X. Y. Zhang, Y. Dai, J. Y. Wei and M. Whangbo, *Angew. Chem., Int. Ed.*, 2008, **47**, 7931-7933.
12 Z. G. Yi, J. H. Ye, N. Kikugawa, T. Kako, S. Ouyang, H. Stuart-Williams, H. Yang, J. Y. Cao, W. J. Luo, Z. S. Li, Y. Liu and R. L. Withers, *Nat. Mater.*, 2010, **9**, 559-564.
13 X.F. Wang, S. F. Li, H. G. Yu, J. G. Yu and S. W. Liu, *Chem. Eur. J.*, 2011, **17**, 7777-7780.
14 J. T. Tang, D. T. Li, Z. X. Feng, Z. Tan and B. L. Ou. *RSC Adv.*, 2014, **4**, 2151-2154.
15 G. P. Dai, J. G. Yu and G. Liu, *J. Phys. Chem. C*, 2012, **116**, 15519-15524.
16 H. J. Dong, G. Chen, J. X. Sun, C. M. Li, Y. G. Yu and D. H. Chen, *Appl. Catal. B*, 2013, **134-135**, 46-54.
17 C. W. Xu, Y. Y. Liu, B. B. Huang, H. Li, X. Y. Qin, X. Y. Zhang and Y. Dai, *Appl. Surf. Sci.*, 2011, **257**, 8732-8736.
18 M. J. Allen, V. C. Tung, R. B. Kaner, *Chem. Rev.*, 2010, **110**, 132-145.
19 Q. J. Xiang, J. G. Yu, M. Jaroniec, *Chem. Soc. Rev.*, 2012, **41**, 782-796.
20 W. G. Wang, J. G. Yu, Q. J. Xiang and B. Cheng, *Appl. Catal. B*, 2012, **119-120**, 109-116.
21 P. Y. Dong, Y. H. Wang, B. C. Cao, S. Y. Xin, L. N. Guo, J. Zhang and F. H. Li. *Appl. Catal. B*, 2013, **132-133**, 45-53.
22 I. V. Lightcap, T. H. Kosel and P. V. Kamat, *Nano Lett.*, 2010, **10**, 577-583.
23 C. Dong, K. L. Wu, X. W. Wei, X. Z. Li, L. Liu, T. H. Ding, J. Wang and Y. Ye, *CrystEngComm*, 2014, **16**, 730-736.
24 N. J. Bell, Y. H.Ng, A. Du, H. Coster, S. C. Smith, and R. Amal, *J. Phys. Chem.* C, 2012, **116**, 18023-18031.
25. F. Meng, J. T. Li, S. K. Cushing, J. Bright, M. J. Zhi, J. D. Rowley, Z. L. Hong, A. Manivannan, A. D. Bristow, and N. Q. Wu, *ACS Catal.*, 2013, **3**, 746-751.
26 J. B. Joo, Q. Zhang, M. Dahl, I. Lee, J. Goebl, F. Zaera, Y. D. Yin, *Energy Environ. Sci.*, 2012, **5**, 6321-6327.
27 Q. Li, B.D. Guo, J.G. Yu, J.R. Ran, B.H. Zhang, H.J. Yan, J.R. Gong, *J. Am. Chem. Soc.*, 2011, **133**, 10878-10884.

28 H.J. Shin, K.K. Kim, A. Benayad, S.M. Yoon, H.K. Park, I.S. Jung, M.H. Jin, H.K. Jeong, J.M. Kim, J.Y. Choi, Y.H. Lee, *Adv. Funct. Mater*., 2009, **19**, 1987-1992.
29 S. Yin, Y. Aita, M. Komatsu, J. Wang, Q. Tang, T. Sato, *J. Mater. Chem*., 2005, **15**, 674-682.
30 Q.J. Xiang and J.G. Yu, *Chinese J. Catal*., 2011, **32**, 525-531.
31 J. Liu, H. Bai, Y. Wang, Z. Liu, X. Zhang and D. D. Sun, *Adv. Funct. Mater*., 2010, **20**, 4175-4181.
32 Q. J. Xiang, J. G. Yu and M. Jaroniec, *Nanoscale*, 2011, **3**, 3670-3678.
33 S. Bai, X. P. Shen, H. W. Lv, G. X. Zhu, C. L. Bao and Y. X. Shan, *J. Colloid Interface Sci*., 2013, 405, 1-9.
34 S. Villar-Rodil, J. I. Paredes, A. Martinez-Alonso and J. M. D. Tascon, *J. Mater. Chem*., 2009, **19**, 3591-3593.
35 H. Wang, J. T. Robinson, X. Li and H. Dai, *J. Am. Chem. Soc.*, 2009, **131**, 9910-9911.

Graphical abstract

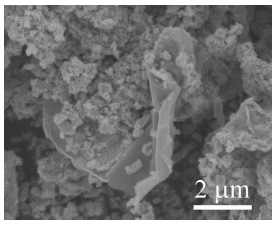

Nano-sized Ag_2CO_3/RGO photocatalysts were fabricated by a facile chemical precipitation approach in DMF solvent. The Ag_2CO_3/RGO nanocomposites exhibited higher photocatalytic activity and stability than the pure nano-sized Ag_2CO_3.